Dalton Transactions

ROYAL SOCIETY OF CHEMISTRY

PAPER

View Article Online
View Journal | View Issue

Cite this: *Dalton Trans.*, 2025, **54**, 16095

Introducing (inter-)halogen polysulfates – a study on the influence of halogen bonding on weakly coordinating anions

Jan Langwald, [a] Rosa M. Gomila, [b] David van Gerven,[a] Antonio Frontera *[b] and Mathias S. Wickleder *[a]

We present the isolation and structural elucidation of the first (inter-)halogen polysulfates $[I_3]_4[S_4O_{13}]_2(SO_3)$, $[IBr_2]_2[S_4O_{13}]$, $[ICl_2][HS_2O_7]$ and $[ICl_2]_2[S_2O_7]$. All compounds are accessible by the reaction of I_2, Br_2 and ICl_3 with neat SO_3 in sealed glass ampoules. The novel compounds show strong donor–acceptor interactions between the oxoanionic polysulfates and the electrophilic central iodine atom of the cations. The strength of the halogen bond increases with electron withdrawal from the iodine. The electron density donation from the polysulfates into the antibonding σ*-molecular orbitals leads to a significant weakening of the X–I bond. The influence of the HaB on the bonding situation within the anions is analyzed and compared to that of $Li_2[S_4O_{13}]$, which we synthesized as a reference alkaline metal polysulfate, showing purely electrostatic cation–anion interactions. Density functional theory (DFT) investigations and resulting MEP surface plots and QTAIM and NBO analyses show the physical nature of the HaB and reveal their energetic driving force. These insights extend our view on the influence of non-covalent interactions on anions we usually call 'weakly coordinating'.

Received 30th August 2025,
Accepted 29th September 2025

DOI: 10.1039/d5dt02088c

rsc.li/dalton

Introduction

The stabilization of highly reactive, thus elusive, (inter-) halogen cations is an ongoing race that was initiated by the work of Gillespie *et al.* in the middle of the last century, who investigated the existence of such species in superacidic systems such as oleum and fluorosulfuric acid.[1–3] Their work was inspired by the well-known observation that selenium dissolves in oleum yielding green solutions. It could be shown that the tetraselenium cation Se_4^{2+} can be isolated from such solutions as the hydrogendisulfate salt $[Se_4][HS_2O_7]$.[4] Interestingly, together with $[Te_6][OTf]_4$ reported by Beck *et al.*,[5] these are the only examples so far for the stabilisation of non-metal polycations by oxoanions. For the stabilization of (inter-) halogen compounds, almost exclusively fluoropnictogenate and -metalate anions were used. The respective weakly coordinating anions (WCA) were not labile to superacidic environments or oxidation and the preparation from available precursors such as IX_n (X = Cl, Br, F; n = 3, 5, 7) *via* Lewis acid (LA) mediated halide abstraction was an efficient synthetic route.[6–9] However, in many cases, either the respective neutral interhalogen compound had to be prepared as a suitable precursor or an additional oxidant was necessary for the generation of the cation.[10–12] With the rise of single crystal X-ray diffraction (SCXRD) techniques, several species were isolated and structurally elucidated by Gillespie ($[I_4]^{2+}$),[13] Passmore ($[I_3]^+$),[9] Birchall ($[ICl_2]^+$),[7] Minkwitz ($[Br_5]^+$)[14] and Kraus ($[Br_2F_5]^+$),[15] besides others. Although these cations were first studied in oleum and the existence of (hydrogen-)polysulfate anions was known, no interhalogen polysulfate has been reported to date. We were able to stabilize the three cations $[I_3]^+$, $[IBr_2]^+$ and $[ICl_2]^+$ in an oxoanionic environment as polysulfates and a hydrogendisulfate (see Fig. 1).

Oxoanions may serve as weakly coordinating anions, and the perchlorate, $[ClO_4]^-$, and triflate ion, $[CF_3SO_3]^-$, are textbook examples. Despite their higher charge, even polysulfates $[S_nO_{3n+1}]^{2-}$ are weak Lewis bases. Throughout the last two decades, we could show that these polysulfates can be prepared up to n = 6 by reactions with neat SO_3. Since SO_3 is a very strong oxidizer, we are able to conduct oxidation reactions where the obtained species are then stabilized by polysulfate anions. A striking example is the disulfate $Pd[S_2O_7]$ which forms almost quantitatively in the reaction of Pd with SO_3.[16] The paramagnetic compound shows the Pd^{2+} ion in a rarely seen octahedral coordination, proving that the $[S_2O_7]^{2-}$ group causes only a weak ligand field splitting. Of course, if strongly Lewis acidic sites are available, the disulfate group can act

[a]*Institute of Inorganic and Materials Chemistry, University of Cologne, Greinstr. 6, 50939 Cologne, Germany. E-mail: mathias.wickleder@uni-koeln.de*
[b]*Universitat de les Illes Balears, Crta de Valldemossa km 7.5, 07122 Palma de Mallorca, Baleares, Spain. E-mail: toni.frontera@uib.es*

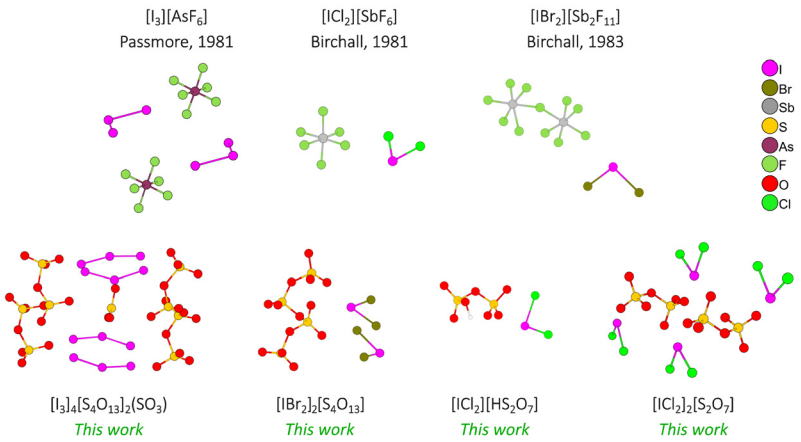

Fig. 1 Summary of the presented structures and literature-known (inter-)halogen compounds.

even as a chelating ligand, as seen in $Te[S_2O_7]_2$ and $ReO_2Cl[S_2O_7]$.[17,18] The possibility of using SO_3 in reactions with highly oxidative species and as a synthon for the formation of weakly basic polysulfate anions encouraged us to investigate the behavior of nonmetals in this medium. In contrast to the above-mentioned fluoropnictogenates and -metalates,[19,20] SO_3 gives a much broader variety of possible reaction conditions, especially with respect to temperature. Indeed, our first attempt, the reaction of elemental iodine with SO_3, yielded the $[I_4]^{2+}$ cation stabilized as a hexasulfate.[21]

In contrast to the fluoropnictogenates, the nature of the polysulfate anions enables the formation of noncovalent interactions towards the cations. One example for these noncovalent interactions is halogen bonding (HaB), a directional noncovalent interaction between an electron-deficient halogen atom (typically bearing a σ-hole) and an electron-rich Lewis base. Conceptually analogous to hydrogen bonding, it belongs to a broader family of σ-hole interactions, which includes chalcogen- (ChB), pnictogen- (PnB), and spodium bonding, among others.[22–27] These interactions generally arise from the approach of a nucleophilic site (a lone pair or π-system) to an electrophilic region along the extension of a covalent bond, the so-called σ-hole.[28,29] This raises the question up to what extent we think of "weakly" coordinating anions, especially when a certain degree of coordination might be the stabilizing factor. Similar considerations were lately discussed by Malischewski and co-workers concerning the perfluorinated Cp* anion, using the term "ambivalent" coordination behaviour.[30]

Although electrostatics provide the dominant driving force, charge-transfer (orbital) interactions play an increasingly recognized role, giving rise to strong directionality.[31] This directionality typically increases with donor electrophilicity and decreases with electronegativity (PnB < ChB < HaB).[32] HaB has been widely studied using neutral organic donors such as aryl or alkyl halides, interacting with common Lewis bases like nitrogen and oxygen donors.[33] These interactions have found broad applications in crystal engineering,[34–38] supramolecular chemistry,[39,40] catalysis,[41–44] and medicinal chemistry.[45–47] Moreover, HaBs can stabilize unusual oxidation states, as exemplified by the Bi(I) complex reported by Malischewski and co-workers.[48] In contrast, the halogen bonding behavior of (inter)halogen cations, such as $[ICl_2]^+$, $[IBr_2]^+$, and $[I_3]^+$, has received limited attention. While recent spectroscopic studies by Bryce and co-workers investigated HaBs in the solid state using aryl-based donors,[49] the potential of small interhalogen cations as HaB donors in the solid state remains largely unexplored. This is particularly noteworthy, as cationic donors such as $[IY_2]^+$ (Y = Cl, Br, I) are expected to exhibit an enhanced σ-hole character and stronger electrostatic interactions compared to neutral species.

Isoelectronic with bent chalcogen species R_2Ch (Ch = O, S, Se, Te), the $[XY_2]^+$ cations possess two σ-holes and can engage in multiple directional HaBs (see Fig. 2). Their potential as building blocks in supramolecular architectures and their role in directing anion coordination *via* noncovalent interactions warrants further investigation. To date, only a few examples of halogen cations stabilized by sulfate-based oxoanionic environ-

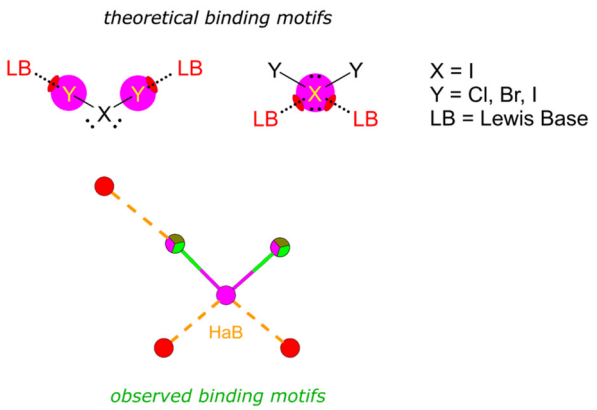

Fig. 2 Theoretical and observed binding motifs for HaB between the (inter-)halogen cations and polysulfate anions.

ments are known. These include iodine(III) bis(fluorosulfate) iodide, $I[OSO_2F]_2I$, reported by Gillespie in 1989,[10] and the first homoatomic halogen polysulfate, $[I_4][S_6O_{19}]$, recently described by our group.[21]

Building on this foundation, we sought to expand the family of polysulfates through the synthesis and structural characterization of new (inter)halogen cation salts stabilized by polysulfate anions. Our goal was to investigate how these highly Lewis acidic cations coordinate to oxoanions and to compare their supramolecular behavior with that of halidopnictogenate systems. To complement the experimental insights, we employed density functional theory (DFT) calculations, including molecular electrostatic potential (MEP) surface analysis, QTAIM, and natural bond orbital (NBO) approaches, to probe the nature and strength of the HaBs observed in the solid state. This combined experimental and theoretical approach provides a detailed understanding of the role of directional σ-hole interactions in stabilizing these species and challenges the classical view of polysulfates as merely weakly coordinating anions.

Results and discussion

For our investigation, we synthesized the first (inter-)halogen tetrasulfate $[IBr_2]_2[S_4O_{13}]$ (**1**), the homoatomic $[I_3]_4[S_4O_{13}]_2(SO_3)$ (**2**) and the first (inter-)halogen (hydrogen-) disulfates $[ICl_2][HS_2O_7]$ (**3**) and $[ICl_2]_2[S_2O_7]$ (**4**), respectively. We were able to generate compounds **1** and **2** directly from reactions of the elements with neat SO_3 under solvothermal conditions in closed glass ampoules. This highlights the efficiency of neat SO_3 for the generation and stabilization of these cationic species since it can act both as an oxidant and a building block for the respective WCAs. Compounds **3** and **4** were generated from I_2Cl_6 as a precursor, with the former one forming after hydrolysis upon exposure to ambient humidity. To compare the influence of HaB on the bond lengths within the anions, we also synthesized the purely ionic lithium polysulfate $Li_2[S_4O_{13}]$ (**5**). Compound **5** was synthesized using lithium bisimide ($Li[NTf_2]$), thus proving that the Brønsted acidity of polysulfuric acids surpasses that of known strong superacids like Tf_2NH.[50] The synthetic procedures and crystallographic details are summarized in the SI.

The compounds with heteroatomic cations **1**, **3** and **4** crystallize with triclinic symmetry (space group $P\bar{1}$, no. 1) and the compounds with homoatomic cations **2** and **5** crystallize in the monoclinic space groups *Cc* (no. 9) and $P2_1/n$ (no.14), respectively. This extends the number of reported main group tetrasulfates that was so far limited to the compounds $[NO_2]_2[S_4O_{13}]$ and $Ba[S_4O_{13}]$.[51,52] All compounds were structurally elucidated *via* SCXRD, where strong donor–acceptor (DA) interactions between the oxoanionic polysulfates and the electrophilic sites of the cations could already be observed by changes in bond lengths and DA distances. Additionally, we performed DFT calculations to analyze the orbital interactions and visualize the halogen bonding. The solid bulk material from which single crystals of **1** and **2** were isolated was investigated using IR and Raman spectroscopy and the results were compared to literature values, as well as the respective modelled spectra using quantum chemical calculations (see the SI, Fig. S13 and S14 and Tables S31–S34). While the vibrational modes of the respective cations for both compounds **1** and **2** found *via* Raman spectroscopy measurements are in good agreement with the literature and calculated values, the vibrational modes of the tetrasulfate anion are only pronounced in the case of **2**. Due to the high reactivity of **3** and **4** and the disadvantage that both compounds could only be isolated from surrounded crystalline SO_3 on a microscope slide with inert oil, no spectroscopic data could be collected for them.

Bonding situation within the anions

In an isolated polysulfate anion, the terminal S–O bonds of all SO_4 units should only differ marginally, mainly possessing a double bond character. Although the negative charge is delocalized over the polysulfate chain, it usually concentrates at the terminal units. This is found in the already published group I and II polysulfates, where the cations are coordinated by all terminal oxygen atoms. Only a small change in the S–O bond length can be observed upon coordination and correlated to the respective O–M (M = Li, Na, K, Ag) distance.[51] The $S–O_{co}$ bond lengths at both ends of the polysulfate chains are usually elongated by 1–3 pm compared to the $S–O_t$ bonds within the chain. The S–O bond lengths within all novel compounds are summarized and compared in Fig. 3. All bond lengths can be found in the SI.

The novel group I tetrasulfate **5** shows all the above-mentioned trends (see the SI, Tables S25–S30 and Fig. S11 and S12). The $S–O_t$ bond lengths range between 140.9(2) and 141.1 (2) pm, while the $S–O_{co}$ bond lengths are slightly elongated

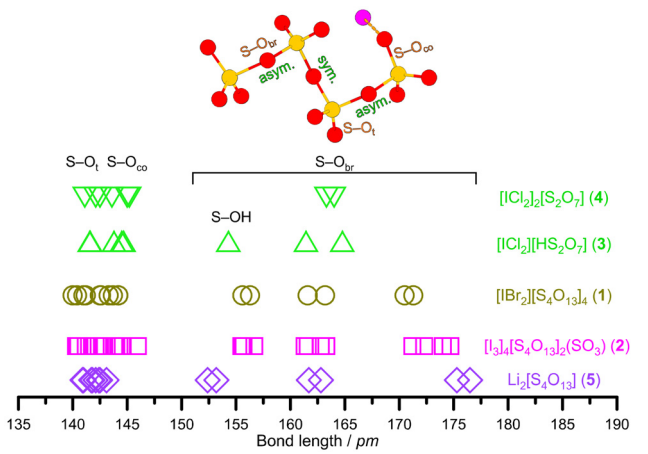

Fig. 3 S–O bond lengths within compounds **1–5**. t = terminal, co = coordinating, br = bridging; sym. = symmetric bridge (similar bond lengths towards both sulfur atoms from the bridging oxygen atom), asym. = asymmetric bridge (alternating bond lengths; short bond length towards the inner sulfur atom and long bond length towards the terminal sulfur atom).

(141.8(2)–143.1(2) pm). Compound **5** shows a bond length asymmetry in the S2–O231–S3 bridge (161.7(2) pm/162.8(2) pm) and the terminal bridges (176.5(2) pm/152.4(2) pm; 175.3 (2) pm/153.2(2) pm). This is in good agreement with the literature-known tetrasulfates and $Li_2[S_5O_{16}]$. Notably, the novel lithium tetrasulfate shows a mixed coordination of the Li atoms, one atom being coordinated tetrahedrally and the other octahedrally by adjacent oxygen atoms. This differs from the exclusively octahedral coordination reported for $Li_2[S_5O_{16}]$.[53] The different coordination environment leads to decreased Li···O distances (188.6(6)–196.6(7) pm) for the tetrahedral coordinated Li1 atom and increased distances (203.8 (7)–218.7(7) pm) for the octahedrally coordinated Li2 atom, which would be expected due to the electrostatic repulsion of approaching oxygen atoms in the octahedral coordination.

The novel (inter-)halogen tetrasulfates **1** and **2** show two major deviations in the S–O bonds. First, the coordinating S–O_{co} bond length increases up to 146(1) pm for **2** and 144.2(3) pm for **1**. They differ strongly from the terminal S–O_t bond lengths, which range between 140(1) and 143(1) pm for **2** and 140.0(3) and 141.2(3) pm for **1**. Furthermore, the S–O_{br} bond length of the terminal O–S bridges decreases significantly down to a minimum of 171.2(9) pm for **2** and 170.5(3) pm for **1**. Simultaneously, the bond lengths of the terminal bridging oxygen atoms towards the inner-lying sulfur atoms slightly increase, which leads to an overall decrease of the asymmetric character of the S–O–S bridges compared to the group I and II tetrasulfates.

The same behavior is observed for compounds **3** and **4** with the $[ICl_2]^+$ cation. Although (hydrogen-)disulfate anions possess only one S–O–S bridge, there is still an asymmetry with one shorter and one longer S–O_{br} bond (usually 5–10 pm), as reported for $M_2[S_2O_7]$ (M = Li, Na, K)[54,55] and M′$[HS_2O_7]$ (M′ = Li, K, Rb, Cs, $[NH_4]$, [NO]) by our group.[56,57] The compounds **3** and **4** show a decreased asymmetry, which basically vanished in the latter case (S1–0121 = 163.3(3) pm; (S2–O121 = 164.0(3) pm). We can clarify the bond length changes by envisioning the formation of polysulfates, starting from the simplest building blocks SO_3 and H_2SO_4 (see Fig. 4).

The S=O double bond within SO_3 ranges from 140 to 141 pm in the γ- and β-modifications reported by Westrik,[58,59] as well as the solid state structures of H_2SO_4 and $H_2S_2O_7$ reported by Hartt and Hönle, respectively.[60,61] The S–O single bond ranges between 151.8(1) pm (FSO_3H),[62] 152.0(5)–152.9(3) pm ($H_2S_2O_7$) and 154 pm (H_2SO_4). Lastly, the dative O–S bond length of the 1,4-dioxane·SO_3 adducts (mono- and diadducts) ranges from 185.0 to 192.8 pm.[63] We suggest that the polysulfate chain growth should be depicted as a subsequent Lewis adduct formation *via* SO_3 addition to a terminal sulfate unit (see Fig. 4a).

Starting from a sulfate ion, $[SO_4]^{2-}$, the oxoanion will form a dative bond with the Lewis acidic sulfur atom of the SO_3 monomer. This bond will be the longest bond, formally being an $O_3SO–SO_3$ dative bond. For tri- and higher polysulfates, the coordinating S–O_{co} bond of the former terminal SO_4 unit will elongate as it transitions from a S–O^- to a S–OR bond. This explains the bond length asymmetry of the S–O–S bridges. Upon complete coordination of a SO_3 unit, the negative charge of the former coordinating S–O^- oxygen atom delocalizes on the new terminal SO_3 unit, leading to a bond length elongation compared to the uncoordinated S=O bonds. This process can proceed until the negative charge on the terminal SO_3 unit of the $[S_nO_{3n+1}]^{2-}$ polysulfate is not Lewis basic enough anymore to add to another SO_3 unit. Until today, this is the case for the hexasulfates. This approach explains the bond length changes upon coordination of a strongly Lewis acidic cation instead of SO_3 (see Fig. 4b). The coordination by an oxygen atom at the terminal SO_3 units of the polysulfate leads

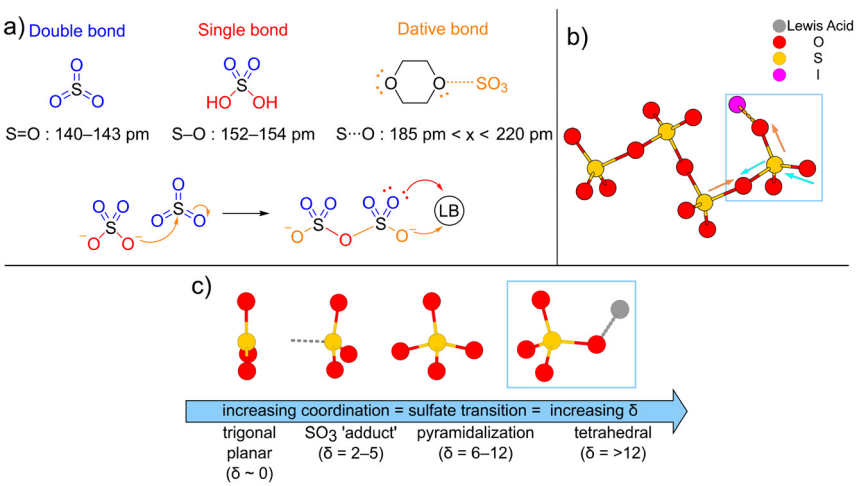

Fig. 4 (a) Bond lengths of common sulfur–oxygen double- (blue), single- (red) and dative bonds (orange). Schematic representation of the polysulfate chain growth *via* dative bond formation between a sulfate unit and a free SO_3 monomer. (b) Bond length changes upon coordination of an oxygen atom of a terminal SO_4 unit to a LA (iodine in the case of compounds **1–4**). Light blue and orange colors indicate a bond length decrease and increase, respectively. (c) Simplified geometric transition process of a SO_3 monomer towards a SO_4 unit and subsequent coordination towards another LA.

to a S–O_{co} bond length increase, thus a slow transition from the S–O^- towards a S–O(R) bond. Subsequently, the electron density withdrawal from the terminal oxygen atoms delocalizes into the polysulfate chain and leads to an overall decrease in the S–O–S bond length asymmetry.

Besides looking at bond lengths, the strength of coordination towards a SO_3 unit can be judged based on its geometry (see Fig. 4c). Monomeric SO_3 shows a perfect trigonal planar geometry with D_{3h} symmetry. Upon coordination (= nucleophilic attack/dative bond formation) of a Lewis base at the central sulfur atom, a transition (distortion) of the trigonal planar geometry towards the tetrahedral geometry of a sulfate unit $[SO_4]^{2-}$ can be observed. In the past, we envisioned using the 'δ parameter' to describe this deviation from the perfect trigonal planar geometry.[64] We herein present an optimized procedure (see the SI) for the measurement of δ values using the software *Polynator*.[65] Fig. 5 shows the δ values as a function of the Lewis base–sulfur (LB–S) bond length for our compounds compared to crystallographically reported main group polysulfates.

The respective bond lengths were extracted from the .cif files. A complete overview of the analyzed structures, the calculated δ values and the bond lengths can be found in the SI (see Table S35). The δ values of **1** already surpass those of $Ca[S_3O_{13}]$ and $Pb[S_3O_{10}]$, although the Lewis basicity of polysulfates usually decreases with increasing chain length. The (hydrogen-)disulfate compounds **3** and **4** show δ values that are in the same regime as $Te[S_2O_7]_2$ and $[ReO_2Cl][S_2O_7]$, which were described as molecular species. This highlights the extreme Lewis acidity of the $[IX_2]^+$ cations. For all compared O–Lewis bases, polysulfates and neutral adducts, the δ values correlate with the LB–S distances. Our findings show that, even if the terminal SO_3 unit of a polysulfate is weakly bound, *i.e.* a long S–O_{br} bond length and a small δ value, the coordination of a strongly Lewis acidic cation leads to increasing pyramidalization and decreasing S–O_{br} bond length. Thus, not only does the anion stabilize the cation, but the cation-induced HaB also stabilizes the anion.

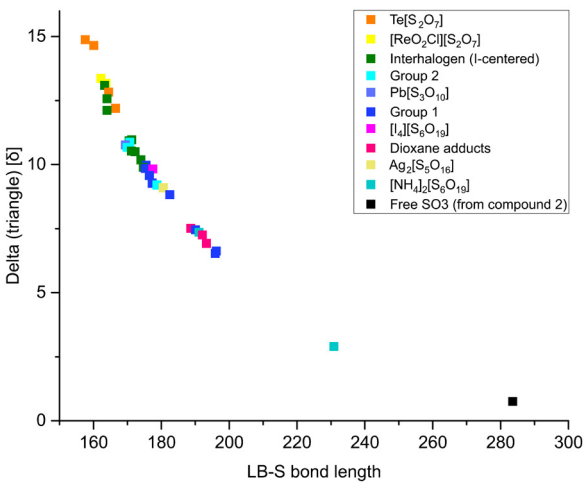

Fig. 5 δ values as a function of the Lewis base–sulfur bond length in pm. A summary of the respective values can be found in the SI.

Bonding situation and coordination of the cations

The DA interactions between the cations and the polysulfate anions can be compared *via* the interatomic distances between the halogen atoms and the oxygen atoms, as well as the bond lengths within the cations (see Fig. 6). Our novel polysulfates show shortened X···O (X = I, Br, Cl) distances compared to the X–F distances in published fluoropnictogenates. For the $[ICl_2]^+$ cation, the reference $[SbCl_6]^-$ and $[AlCl_4]^-$ compounds are not suitable for comparison since an equilibrium between $[ICl_2]^+$ and $[ICl_4]^-$ was proposed for these species, leading to deviations in the I–Cl bond lengths.[6]

The central iodine atom is expected to be the most electrophilic site in the cations, as Schwarz and co-workers showed using DFT calculations.[66] Thus, when moving from $[I_3]^+$ to $[IBr_2]^+$ and $[ICl_2]^+$, the polarization and electron density withdrawal from the central atom increase and the DA interactions become stronger. This is exactly what the I···O distances for compounds **1–4** show. If the shortest I···O distances are compared, they decrease from 262(1) pm (**2**) over 260.1(4) pm (**1**) and 258.1(7) pm (**3**) down to 244.0(5) pm (**4**), which relates to the increasing Lewis basicity of the shorter disulfates compared to the tetrasulfates. Notably, the I···O distances towards the terminal I atoms in compound **2** are shorter, which would be counter-intuitive at first but can be clarified by quantum chemical analysis of the cation, which will be provided in the following chapter. Furthermore, it shows the weaker Lewis basicity of the single protonated $[HS_2O_7]^-$ compared to the $[S_2O_7]^{2-}$ anion. For compound **4**, the difference between the longest I–Cl bond and the shortest I···O distance is only 14 pm, highlighting that the border between classic covalency and strong non-covalent interactions is reached.

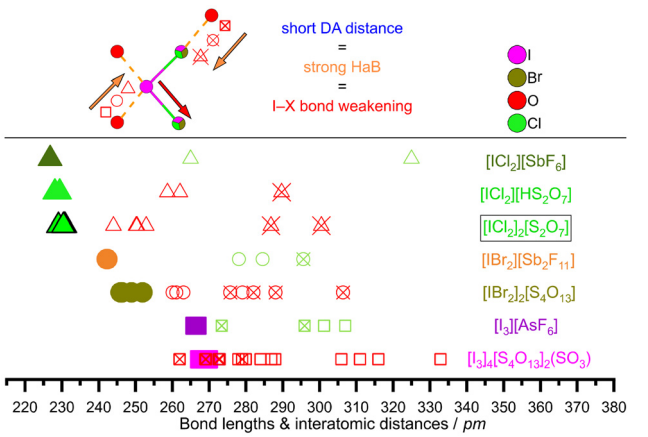

Fig. 6 Bond lengths within the cations (solid symbols) and interatomic distances towards the next coordinating donor atom of the respective anion (open symbols). Open symbols with a cross represent coordination towards the terminal halogen atoms of the cation. Red and green colors of the open symbols represent oxygen and fluorine atoms, respectively.

With decreasing DA distances, the opposite halogen–halogen bond length increases. This bond elongation is already considerable for the $[I_3]^+$ and $[ICl_2]^+$ cations in **2** and **3** (up to 1.5% compared to the $[PnF_6]^-$ compounds (Pn = Sb, As)). It increases significantly for the cations in **1** and **4** (up to 1.8 and 4%, respectively). Especially in case of **1** ($[IBr_2]^+$), the decreased DA distance and the increased I–Br bond length indicates an HaB induced I–Br bond weakening due to partial occupation of the σ*-orbital *via* electron density donation of the oxoanions. In contrast to the published calculations, the shortest DA distances in compound **2**, as well as the reference compound $[I_3][AsF_6]$, are not formed between the central iodine atoms but between the terminal iodine atoms (see the SI, Fig. S6). The spatial approximation of the donor atoms and resulting elongation of the I–X bonds lead to a geometric transition of the $[IX_2]^+$ species (see Table 1).

When the HaB between the anions and the cations becomes stronger, the resulting X–I–D angles increase, resulting in a transition of the former bent geometry of $[IX_2]^+$ (X = I, Br, Cl) towards a formally square-planar $D_2[IX_2]^+$ species. This effect becomes stronger when the central iodine atom gets more electrophilic, *i.e.* when moving from $[I_3]^+$ to $[ICl_2]^+$. The shorter the D–I distances are, the stronger the HaB becomes and thus the longer gets the opposite I–X bond. Since the electrostatic repulsion is smaller between oxygen atoms than between halogen atoms, the A angle for the oxoanionic compounds is smaller compared to the fluoropnictogenates. Simultaneously, the increasing I–X bond length results in a weakened electrostatic repulsion of the terminal halogen atoms in the cation. Thus, the B angle approximates towards 90° compared to the free cations. The deviation from the calculated values increases from $[I_3]^+$ to $[ICl_2]^+$, which shows the influence of stronger HaB on the bond weakening and thus the geometric transition.

The high directionality of HaB is a result of the electron density donation into the I–X bond's σ*-molecular orbital. The directionality and strength of HaB are therefore interrelated. This is equal to other non-covalent interactions like hydrogen bonding (HB), where the O–H–donor angle is used for classification of the strength.[23] Our compounds show increased C angles compared to the reference compounds, indicating an increased HaB towards our anions compared to the fluoropnictogenates. For the heteroatomic compounds **1**, **3** and **4**, the strongest HaB is found for the oxygen atoms that coordinate to the central iodine atom of the cations, whereas the oxygen atoms that coordinate to the terminal Br and Cl atoms lead to the C angles below 170° (see the SI, Fig. S4, S8 and S10).

The aforementioned effects should further increase when moving from $[ICl_2]^+$ to the even more electrophilic $[IF_2]^+$ cation. To our knowledge, there has been no reported crystal structure with this cation; only the higher fluorinated $[IF_4]^+$ and $[IF_6]^+$ cations have been isolated using fluoropnictogenates.[11,67–69] The (an)ion affinity of any Lewis acid increases with its strength, resulting in the ability of super LAs to abstract even weak anionic leaving groups like H^- and F^-.[70–72] Although the significant increase in fluoride ion affinity (FIA) for cationic group V LAs has been reported, no calculation has been made for cationic group VII species to date.[73,74] It thus might be that $[IF_2]^+$ is so Lewis acidic that it leads to covalent bound (poly-)sulfate compounds, which would not be ionic anymore but show a covalent F_2I–OS bond. Gillespie and his colleagues already described the central iodine atom of $I[OSO_2F]_2I$ as weakly covalently bound to fluorosulfate ligands, judged by the short I···O distance of 208.6(7) pm to 225.8(8) pm.[10] For our systems, compound **4** already shows I···O distances below 250 pm. The loss of stabilizing lattice energy in molecular compounds complicates crystallization and might be one reason for the absence of crystal struc-

Table 1 Summary of the D–I–D (A), X–I–X (B) and X–I–D (C) angles within compounds **1–4** compared to reference compounds and the calculated data for the trihalogen cluster cations. In an ideal square-planar coordination of the central I atom, the A, B and C angles would be 90°, 90° and 180°, respectively

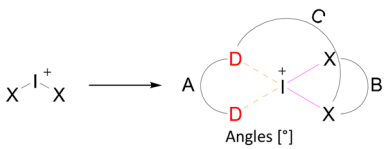

	Angles [°]			
Compound	A	B	C	Ref.
$[I_3]_4[S_4O_{13}]_2(SO_3)$ (**2**)	97.32(3)–102.51(3)	82.6(3)–103.3(3)	161.5(2)–177.4(2)	This work
$[I_3][AsF_6]$	101.6(4)	101.8(4)	170.8(3)–174.8(3)	9
$[I_3]^+$	—	101	—	66
$[IBr_2]_2[S_4O_{13}]$ (**1**)	92.2(1)–98.4(1)	96.4(1)–99.3(1)	161.2(6)–177.8(7)	This work
$[IBr_2][Sb_2F_{11}]$	100.0(1)	85.6(4)	157.7(3)–174.3(3)	8
$[IBr_2]^+$	—	100	—	66
$[ICl_2][HS_2O_7]$ (**3**)	101.1(1)	98.9(2)	174.2(1)–178.1(1)	This work
$[ICl_2]_2[S_2O_7]$ (**4**)	99.1(2)–106.4(1)	91.5(4)–94.5(5)	162.9(8)–177.1(1)	This work
$[ICl_2][SbF_6]$	97.2(1)	91.3(2)	169.4(1)	7
$[ICl_2]^+$	—	99	—	66

tures with this motif. We strive towards the isolation of $[IF_n]^+$ (n = 2, 4, 6) polysulfates for the future, especially to study their HaB compared to the herein presented structures.

Quantum chemical calculations

DFT calculations were carried out to investigate the HaB interactions in compounds **1–4**.

Fig. 7 presents selected assemblies of the four compounds, offering key insights into the significance of directional HaBs in solid-state structures.

In compound **1**, the formation of a supramolecular macrocycle is observed, where two tetrasulfate anions are bridged by two $[IBr_2]^+$ cations *via* short I···O HaBs (~260 pm). In compound **2**, a supramolecular cage is formed by the interaction of two tetrasulfate anions with four $[I_3]^+$ cations *via* eight HaBs, where I···O distances are shorter than the sum of van der Waals radii ($\sum R_{vdW}$(I + O) = 350 pm) but longer than the sum of covalent radii ($\sum R_{cov}$(I + O) = 205 pm). A remarkable feature of this structure is the encapsulation of a SO_3 molecule within the $[I_3]_4[S_4O_{13}]_2$ supramolecular cage, allowing structural characterization of this highly reactive gaseous species by X-ray diffraction. Notably, the SO_3 molecule is stabilized by two S···O π-hole chalcogen bonding (ChB) interactions. For compounds **3** and **4**, the $[ICl_2]^+$ cations participate in three concurrent HaBs (see Fig. 7c and d). Compound **4** forms assemblies that are similar to those of compound **1** where two disulfate anions are connected by two cations through I···O HaBs, forming the supramolecular macrocycle 'A'. Additionally, two A rings are further linked *via* Cl···O HaBs, giving rise to macrocycle 'B'. The shortening of the I···O contacts in the solid-state structures already indicates that the HaB strength within the $[IX_2]^+$ species follows the order X = Cl > Br > I. This aspect was further explored in the theoretical study, where the nature of the HaB and ChB interactions was analyzed. First, the MEP surfaces of the SO_3 molecule and $[IX_2]^+$ cations (shown in two different views) were computed (see Fig. 8) to rationalize the X-ray structures described before.

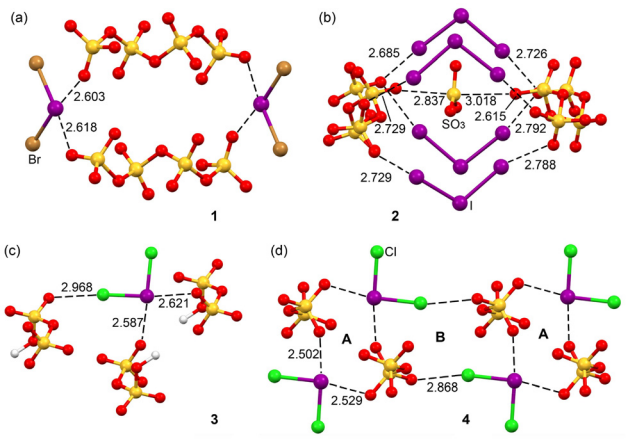

Fig. 7 Partial views of the X-ray packing of compounds **1** (a), **2** (b), **3** (c) and **4** (d). Halogen (σ-hole) and chalcogen (π-hole) bonds are represented as dashed lines. Distances in Å.

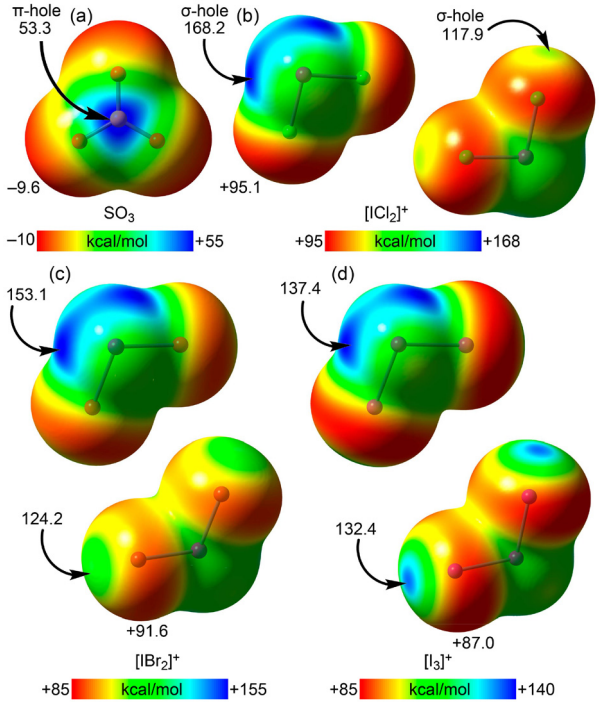

Fig. 8 MEP surfaces of SO_3 (a), $[ICl_2]^+$ (b), $[IBr_2]^+$ (c) and $[I_3]^+$ (d). The MEP values at selected points of the surfaces are given in kcal mol^{-1} (isosurface 0.001 a.u.).

For the SO_3 neutral molecule, the MEP surface reveals two intense π-holes (53.3 kcal mol^{-1}) positioned above and below the central sulfur atom, explaining its high electrophilicity. The MEP minima are located at the oxygen atoms, with a value of −9.6 kcal mol^{-1}, revealing very low nucleophilicity. This strong anisotropy in electron density distribution explains the formation of double π-hole interactions in compound **2**. The MEP values for the cationic $[IX_2]^+$ species (see Fig. 8b–d) are positive across the entire van der Waals surface. The distribution is also anisotropic, exhibiting significant variations along the surface. In all cases, two intense σ-holes are located at the central iodine atom, where the MEP values reach their maximum. The least polarized cation $[I_3]^+$ shows only a small difference in the MEP between the central and the terminal iodine atoms, which explains the counter-intuitive trend of short I···O distances towards the terminal atoms discussed previously.

The MEP maximum decreases as the halogen becomes heavier ($V_{s,max}$ = 168.2 kcal mol^{-1} for Cl, 153.1 kcal mol^{-1} for Br, and 137.4 kcal mol^{-1} for I), explaining the shorter I···O distances observed in compounds **3** and **4**. Additionally, the presence of local maxima at the X-atoms of the $[IX_2]^+$ cations is noteworthy, whereby the positive potential increases with the heavier halogens. In $[I_3]^+$, the σ-holes at the central iodine atom exhibit nearly the same MEP value as those at the monovalent iodine atoms. This σ-hole distribution accounts for the highly directional HaBs observed in the solid-state structures of compounds **1–4**. To further visualize the influence of the

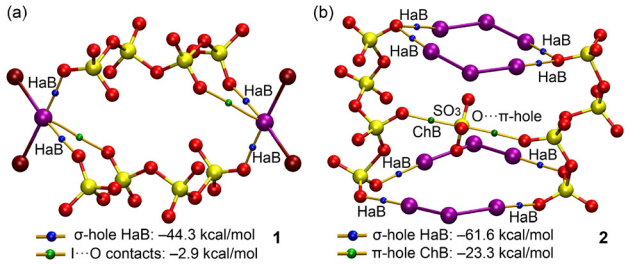

Fig. 9 QTAIM distribution of BCPs (small spheres) and bond paths (orange lines) for compounds **1** (a) and **2** (b). Only intermolecular BCPs characterizing ChB and HaBs are represented for clarity.

noncovalent interactions on the macromolecular arrangement, we used the quantum theory of atoms in molecules (QTAIM) analysis.

Fig. 9 presents the distribution of bond critical points (BCPs) (small spheres) and bond paths (orange lines) for compounds **1** and **2**.

In compound **1**, each $[IBr_2]^+$ cation forms two strong HaBs, characterized by blue BCPs. The formation energy of the supramolecular cage was computed using the potential energy densities at the BCPs, following the approach proposed by Tsirelson.[75] The total interaction energy associated with these HaBs is −44.3 kcal mol^{-1} for four contacts, confirming the strong bonding nature and the superior ability of $[IBr_2]^+$ as a σ-hole donor. QTAIM identifies two additional, symmetrically equivalent BCPs (in dark green) and bond paths linking the I atoms to the anions. Due to their lack of directionality, these I···O contacts cannot be classified as HaBs (σ-hole interactions). Instead, they represent nondirectional ion-pair interactions. The computed strength of these I···O contacts is only −2.9 kcal mol^{-1}, significantly weaker than the HaBs. These nondirectional ion-pair interactions are a unique feature of our polysulfate systems since they are formed between innerlying terminal oxygen atoms of the polysulfate chain that are neither available in fluoropnictogenate systems nor in triflates.

For the assembly of compound **2**, each HaB is defined by a BCP (blue) and a bond path linking the terminal I and O atoms. This results in a formation energy of −61.6 kcal mol^{-1} for eight contacts. Notably, QTAIM confirms the presence of chalcogen bonds (dark green), namely π-hole interactions, as evidenced by a BCP and bond path connecting the central S atom of the free SO_3 molecule and inner-lying terminal O atoms of the polysulfate chain. The encapsulation of the SO_3 molecule within the cage was further analyzed using the supramolecular approach at the RI-PBE0-D4/def2-TZVP level of theory. Scalar relativistic effects were included in the ECPs for iodine atoms (for Computational details see SI). The calculated encapsulation energy of −23.3 kcal mol^{-1} shows the significant strength of the π-hole interactions involved in stabilizing the SO_3 molecule.

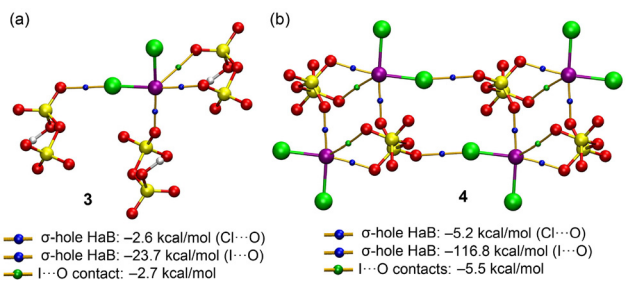

Fig. 10 QTAIM distribution of BCPs (small spheres) and bond paths (orange lines) for compounds **3** (a) and **4** (b). Only intermolecular BCPs characterizing the HaBs are represented for clarity.

Fig. 10 presents the QTAIM analysis for the assemblies of the $[ICl_2]^+$ compounds **3** and **4**. For both compounds, the HaBs are represented by dark blue spheres, while nondirectional I···O contacts are indicated by dark green spheres. The hydrogen disulfate **3** shows two types of HaBs: those involving the σ-holes on iodine atoms (I···O) and those involving the σ-holes on chlorine atoms (Cl···O). Consistent with the MEP analysis and the differences in σ-hole intensity, the Cl···O HaB is modest, with an interaction energy of −2.6 kcal mol^{-1}, whereas the I···O HaBs are significantly stronger, with a total interaction energy of −23.7 kcal mol^{-1} for two contacts. The nondirectional I···O contact is weaker, with an interaction energy of −2.7 kcal mol^{-1}, further underscoring the dominance of I···O HaBs in stabilizing the assembly.

Although a similar general trend is observed in the assembly of the compound **4**, the calculated energies highlight the significant difference between a hydrogendisulfate and a disulfate anion. The I···O HaBs exhibit a very strong interaction energy of −116.8 kcal mol^{-1} for eight contacts. The Cl···O HaBs are significantly weaker, with an interaction energy of −5.2 kcal mol^{-1} for two contacts. Additionally, four nondirectional I···O contacts are observed, with a combined interaction energy of −5.5 kcal mol^{-1}. Overall, the energetic analysis confirms the ranking of HaB donor strength within the $[IX_2]^+$ species, following the order X = Cl > Br > I. Moreover, in all salts, the HaBs involving the central iodine atom are significantly stronger than those involving the terminal halogen atoms, reinforcing the key role of iodine-based σ-hole interactions in stabilizing these assemblies. The identified nondirectional ion-pair interactions, though being weaker than the HaBs, highlight the increased stabilization potential of our systems due to small energetic contributions *via* the chelation by the terminal oxygen atoms of the polysulfate chain. Finally, Natural Bond Orbital (NBO) analysis was performed for a representative set of HaBs to investigate the interactions from an orbital donor–acceptor perspective. The results are summarized in Fig. 11, where the NBOs characterizing the HaBs are depicted.

For compound **1**, the typical LP(O) → σ*(I–Br) electron donation is observed for both types of I···O HaBs. The corresponding stabilization energies due to donor–acceptor electron transfer are 7.3 and 6.4 kcal mol^{-1} for both I···O contacts (see Fig. 11a), indicating a significant contribution of orbital effects to the HaBs. This is directly correlated with the short I···O distances, which allow for efficient orbital overlap between the donor and acceptor orbitals.

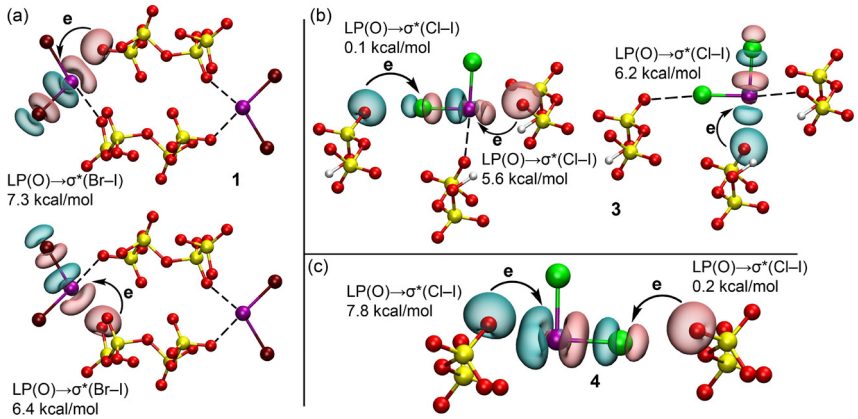

Fig. 11 NBOs involved in the HaBs of compounds **1** (a), **3** (b) and **4** (c). The second order stabilization energies are indicated.

In the case of the hydrogen disulfate **3** (see Fig. 11b), the LP(O) → σ*(I–Cl) electron donation is 5.6 kcal mol^{-1} at the iodine end of the σ*(I–Cl) orbital, while the contribution at the chlorine end is almost negligible (0.1 kcal mol^{-1}). A similar trend is observed for the disulfate **4** (see Fig. 11c), where the LP(O) → σ*(I–Cl) electron donation is notably stronger at the iodine end of the antibonding orbital (7.8 kcal mol^{-1}) compared to the chlorine end (0.2 kcal mol^{-1}). This difference is directly related to the longer Cl···O distance observed in the crystal structure. This NBO analysis further confirms the σ-hole nature of the interaction and highlights the significant role of orbital effects in stabilizing the HaB assemblies.

Conclusion

In this work, we have synthesized and structurally characterized a new series of (inter)halogen polysulfate salts featuring $[ICl_2]^+$, $[IBr_2]^+$, and $[I_3]^+$ cations. We were able to synthesize all compounds in a single step using either neat elements or easily available precursors. Single-crystal X-ray diffraction analysis reveals that these cationic halogen species engage in highly directional halogen bonding interactions with the surrounding oxoanionic polysulfate frameworks. These interactions play a critical role in directing the supramolecular organization of the salts, giving rise to macrocyclic assemblies, extended networks, and even discrete cage-like architectures. Based on thorough structural analysis, we were able to show the correlations between the interionic distances (*i.e.* cation–anion interactions) and the bond length changes within each ion. We used these results to correlate the bond lengths within literature-known polysulfates and our new compounds with the geometry of the terminal SO_3 units and (re-)introduced the δ parameter for this description.

To further understand the nature of these interactions, we performed a comprehensive DFT study employing MEP surface analysis, and QTAIM and NBO calculations. These results confirm the presence of pronounced σ-holes on the iodine centers of the $[IX_2]^+$ cations and support the interpretation of the short I···O contacts as *bona fide* HaBs. The theoretical findings also highlight the ability of the polysulfate anions, typically considered weakly coordinating, to act as effective HaB acceptors through their oxygen lone pairs. We were able to identify additional nondirectional ion-pair interactions as a distinct feature of our anions that contribute to the overall stabilization of the highly reactive cationic species.

Taken together, this study expands the scope of halogen bonding to include interhalogen cation donors in oxoanionic environments and demonstrates how directional σ-hole interactions can be harnessed in the design of complex supramolecular assemblies. These results also open the door to further exploration of polysulfate chemistry beyond classical ionic frameworks, particularly in the context of noncovalent interaction-driven crystal engineering.

Conflicts of interest

There are no conflicts to declare.

Data availability

The data supporting this article (synthetic procedure, crystallographic details, spectroscopic data and computational details) have been included as part of the supplementary information (SI). Supplementary information is available. See DOI: https://doi.org/10.1039/d5dt02088c.

CCDC 2405908 (**1**), 2405913 (**2**), 2405909 (**3**), 2405912 (**4**) and 2405910 (**5**) contain the supplementary crystallographic data for this paper.[76a–e]

Acknowledgements

The authors would like to thank Silke Kremer for the SCXRD measurements and Katrin Eppers for the Raman spectroscopy measurements. J. L. is thankful to the German Academic Scholarship Foundation for financial support.

References

1 R. Gillespie and J. Milne, *Inorg. Chem.*, 1966, **5**, 1577–1582.
2 R. J. Gillespie, J. B. Milne and M. J. Morton, *Inorg. Chem.*, 1968, **7**, 2221–2225.
3 R. J. Gillespie and K. Malhotra, *Inorg. Chem.*, 1969, **8**, 1751–1756.
4 I. D. Brown, D. B. Crump and R. J. Gillespie, *Inorg. Chem.*, 1971, **10**, 2319–2323.
5 C. Schulz, J. Daniels, T. Bredow and J. Beck, *Angew. Chem., Int. Ed.*, 2016, **55**, 1173–1177.
6 C. G. Vonk and E. H. Wiebenga, *Acta Crystallogr.*, 1959, **12**, 859–866.
7 T. Birchall and R. D. Myers, *Inorg. Chem.*, 1981, **20**, 2207–2211.
8 T. Birchall and R. D. Myers, *Inorg. Chem.*, 1983, **22**, 1751–1756.
9 J. Passmore, G. Sutherland and P. S. White, *Inorg. Chem.*, 1981, **20**, 2169–2171.
10 T. Birchall, G. Denes, R. Faggiani, C. S. Frampton, R. J. Gillespie, R. Kapoor and J. E. Vekris, *Inorg. Chem.*, 1990, **29**, 1527–1530.
11 A. J. Edwards and P. Taylor, *J. Chem. Soc., Dalton Trans.*, 1975, 2174–2177, DOI: 10.1039/DT9750002174.
12 R. J. Gillespie and M. J. Morton, *Q. Rev., Chem. Soc.*, 1971, **25**, 553–570.
13 R. Faggiani, R. Gillespie, R. Kapoor, C. Lock and J. Vekris, *Inorg. Chem.*, 1988, **27**, 4350–4355.
14 H. Hartl, J. Nowicki and R. Minkwitz, *Angew. Chem.*, 1991, **103**, 311–312.
15 S. I. Ivlev, A. J. Karttunen, M. R. Buchner, M. Conrad and F. Kraus, *Angew. Chem., Int. Ed.*, 2018, **57**, 14640–14644.
16 J. Bruns, M. Eul, R. Pöttgen and M. S. Wickleder, *Angew. Chem., Int. Ed.*, 2012, **51**, 2204–2207.
17 C. Logemann, J. Bruns, L. V. Schindler, V. Zimmermann and M. S. Wickleder, *Z. Anorg. Allg. Chem.*, 2015, **641**, 831–837.
18 U. Betke, W. Dononelli, T. Klüner and M. S. Wickleder, *Angew. Chem., Int. Ed.*, 2011, **50**, 12361–12363.
19 F. Schrötter and B. G. Müller, *Z. Anorg. Allg. Chem.*, 1993, **619**, 1431–1440.
20 B. Koch, T. Graubner, A. J. Karttunen and F. Kraus, *Eur. J. Inorg. Chem.*, 2024, e202400767.
21 D. van Gerven, S. Sutorius, J. Bruns and M. S. Wickleder, *ChemistryOpen*, 2022, **11**, e202200122.
22 G. R. Desiraju, P. S. Ho, L. Kloo, A. C. Legon, R. Marquardt, P. Metrangolo, P. Politzer, G. Resnati and K. Rissanen, *Pure Appl. Chem.*, 2013, **85**, 1711–1713.
23 T. Steiner, *Angew. Chem., Int. Ed.*, 2002, **41**, 48–76.
24 L. Vogel, P. Wonner and S. M. Huber, *Angew. Chem., Int. Ed.*, 2019, **58**, 1880–1891.
25 S. Zahn, R. Frank, E. Hey-Hawkins and B. Kirchner, *Chem. – Eur. J.*, 2011, **17**, 6034–6038.
26 K. T. Mahmudov, A. V. Gurbanov, V. A. Aliyeva, G. Resnati and A. J. L. Pombeiro, *Coord. Chem. Rev.*, 2020, **418**, 213381.
27 A. Bauzá, I. Alkorta, J. Elguero, T. J. Mooibroek and A. Frontera, *Angew. Chem., Int. Ed.*, 2020, **59**, 17482–17487.
28 V. Angarov and S. Kozuch, *New J. Chem.*, 2018, **42**, 1413–1422.
29 M. H. Kolar and P. Hobza, *Chem. Rev.*, 2016, **116**, 5155–5187.
30 R. Sievers, M. Sellin, S. M. Rupf, J. Parche and M. Malischewski, *Angew. Chem., Int. Ed.*, 2022, **61**, e202211147.
31 B. Pinter, N. Nagels, W. A. Herrebout and F. De Proft, *Chem. – Eur. J.*, 2013, **19**, 519–530.
32 A. Bauzá, T. J. Mooibroek and A. Frontera, *ChemPhysChem*, 2015, **16**, 2496–2517.
33 G. Cavallo, P. Metrangolo, R. Milani, T. Pilati, A. Priimagi, G. Resnati and G. Terraneo, *Chem. Rev.*, 2016, **116**, 2478–2601.
34 R. B. Walsh, C. W. Padgett, P. Metrangolo, G. Resnati, T. W. Hanks and W. T. Pennington, *Cryst. Growth Des.*, 2001, **1**, 165–175.
35 T.-N. Streit, J. Langwald, R. M. Gomila, A. Frontera and M. Malischewski, *CrystEngComm*, 2024, **26**, 3627–3633.
36 J. Teyssandier, K. S. Mali and S. De Feyter, *ChemistryOpen*, 2020, **9**, 225–241.
37 C. B. Aakeröy, T. K. Wijethunga, J. Desper and M. Đaković, *Cryst. Growth Des.*, 2015, **15**, 3853–3861.
38 A. Mukherjee, S. Tothadi and G. R. Desiraju, *Acc. Chem. Res.*, 2014, **47**, 2514–2524.
39 P. Metrangolo, F. Meyer, T. Pilati, G. Resnati and G. Terraneo, *Angew. Chem., Int. Ed.*, 2008, **47**, 6114–6127.
40 R. Kampes, S. Zechel, M. D. Hager and U. S. Schubert, *Chem. Sci.*, 2021, **12**, 9275–9286.
41 R. L. Sutar and S. M. Huber, *ACS Catal.*, 2019, **9**, 9622–9639.
42 D. Bulfield and S. M. Huber, *Chem. – Eur. J.*, 2016, **22**, 14434–14450.
43 Y.-C. Chan and Y.-Y. Yeung, *Angew. Chem., Int. Ed.*, 2018, **57**, 3483–3487.
44 L. Yi, D. Kong, A. Prabhakar Kale, R. Alshehri, H. Yue, A. Gizatullin, B. Maity, R. Kancherla, L. Cavallo and M. Rueping, *Angew. Chem., Int. Ed.*, 2024, **63**, e202411961.
45 M. R. Scholfield, C. M. V. Zanden, M. Carter and P. S. Ho, *Protein Sci.*, 2013, **22**, 139–152.
46 R. Wilcken, M. O. Zimmermann, A. Lange, A. C. Joerger and F. M. Boeckler, *J. Med. Chem.*, 2013, **56**, 1363–1388.
47 E. Margiotta, S. C. C. van der Lubbe, L. de Azevedo Santos, G. Paragi, S. Moro, F. M. Bickelhaupt and C. Fonseca Guerra, *J. Chem. Inf. Model.*, 2020, **60**, 1317–1328.
48 L. P. Griffin, T.-N. Streit, R. Sievers, S. Aldridge, R. M. Gomila, A. Frontera and M. Malischewski, *J. Am. Chem. Soc.*, 2024, **146**, 29877–29882.
49 A. Nari, M. Rahman, P. M. J. Szell, V. Semeniuchenko and D. L. Bryce, *J. Am. Chem. Soc.*, 2025, **147**, 9528–9543.
50 R. Kanzaki, T. Hidaka, Y. Tokuda, H. Kodamatani and T. Tomiyasu, *J. Mol. Liq.*, 2024, **409**, 125433.
51 C. Logemann, T. Klüner and M. S. Wickleder, *Angew. Chem., Int. Ed.*, 2012, **51**, 4997–5000.

52 J. Bruns, L. V. Schindler and M. S. Wickleder, *Z. Anorg. Allg. Chem.*, 2014, **640**, 2345–2345.
53 L. V. Schindler, M. Struckmann, A. Becker and M. S. Wickleder, *Eur. J. Inorg. Chem.*, 2017, **2017**, 958–964.
54 C. Logemann, J. Witt and M. S. Wickleder, *Z. Kristallogr. - New Cryst. Struct.*, 2013, **228**, 159–160.
55 K. Ståhl, T. Balic-Zunic, F. da Silva, K. Michael Eriksen, R. W. Berg and R. Fehrmann, *J. Solid State Chem.*, 2005, **178**, 1697–1704.
56 L. V. Schindler, M. Daub, M. Struckmann, A. Weiz, H. Hillebrecht and M. S. Wickleder, *Z. Anorg. Allg. Chem.*, 2015, **641**, 2604–2609.
57 L. V. Schindler and M. S. Wickleder, *New J. Chem.*, 2017, **41**, 56–62.
58 R. Westrik and C. H. Mac Gillavry, *Recl. Trav. Chim. Pays-Bas*, 1941, **60**, 794–810.
59 R. Westrik, *Acta Crystallogr.*, 1954, **7**, 764–767.
60 A. R. Moodenbaugh, J. E. Hartt, J. J. Hurst, R. W. Youngblood, D. E. Cox and B. C. Frazer, *Phys. Rev. B: Condens. Matter Mater. Phys.*, 1983, **28**, 3501–3505.
61 W. Hönle, *Z. Kristallogr.*, 1991, **196**, 279–288.
62 K. Bartmann and D. Mootz, *Acta Crystallogr., Sect. C: Cryst. Struct. Commun.*, 1990, **46**, 319–320.
63 L. Richtera, J. Taraba and J. Toužín, *Collect. Czech. Chem. Commun.*, 2006, **71**, 155–163.
64 L. V. Schindler, A. Becker, M. Wieckhusen, T. Klüner and M. S. Wickleder, *Angew. Chem., Int. Ed.*, 2016, **55**, 16165–16167.
65 L. Link and R. Niewa, *J. Appl. Crystallogr.*, 2023, **56**, 1855–1864.
66 J. Li, S. Irle and W. E. Schwarz, *Inorg. Chem.*, 1996, **35**, 100–109.
67 E. Goreshnik and Z. Mazej, *Acta Crystallogr., Sect. C:Cryst. Struct. Commun.*, 2006, **62**, i59–i60.
68 J. F. Lehmann, G. J. Schrobilgen, K. O. Christe, A. Kornath and R. J. Suontamo, *Inorg. Chem.*, 2004, **43**, 6905–6921.
69 A. Vij, F. S. Tham, V. Vij, W. W. Wilson and K. O. Christe, *Inorg. Chem.*, 2002, **41**, 6397–6403.
70 H. Böhrer, N. Trapp, D. Himmel, M. Schleep and I. Krossing, *Dalton Trans.*, 2015, **44**, 7489–7499.
71 P. Erdmann, J. Leitner, J. Schwarz and L. Greb, *ChemPhysChem*, 2020, **21**, 987–994.
72 L. M. Sigmund, S. S. V. Sowndarya, A. Albers, P. Erdmann, R. S. Paton and L. Greb, *Angew. Chem., Int. Ed.*, 2024, **63**, e202401084.
73 L. Greb, *Chem. – Eur. J.*, 2018, **24**, 17881–17896.
74 A. P. M. Robertson, P. A. Gray and N. Burford, *Angew. Chem., Int. Ed.*, 2014, **53**, 6050–6069.
75 E. V. Bartashevich and V. G. E. Tsirelson, *Russ. Chem. Rev.*, 2014, **83**, 1181.
76 (*a*) CCDC 2405908: Experimental Crystal Structure Determination, 2025, DOI: 10.5517/ccdc.csd.cc2lrjyv; (*b*) CCDC 2405913: Experimental Crystal Structure Determination, 2025, DOI: 10.5517/ccdc.csd.cc2lrk31; (*c*) CCDC 2405909: Experimental Crystal Structure Determination, 2025, DOI: 10.5517/ccdc.csd.cc2lrjzw; (*d*) CCDC 2405912: Experimental Crystal Structure Determination, 2025, DOI: 10.5517/ccdc.csd.cc2lrk20; (*e*) CCDC 2405910: Experimental Crystal Structure Determination, 2025, DOI: 10.5517/ccdc.csd.cc2lrk0y.